"Revisiting the causal factors of seismicity in the Dallas–Fort Worth area"

Appendix and supplemental material

Iason Grigoratos[1*], Alexandros Savvaidis[2], Heather R. DeShon[3], Stefan Wiemer[1]

[1] Swiss Seismological Service, ETH Zurich (previously)
[2] Bureau of Economic Geology, University of Texas at Austin
[3] Dept. of Earth Sciences, Southern Methodist University
* research@grigoratos.com

Appendix A

A.1 Unified earthquake catalog

Table S1. Sources of parametric earthquake data for the DFW basin in our earthquake catalog.

Source	Time-period		Magnitude Scale	Region/State	M ≥
ComCat (ANSS)	2000	Feb 2023	varied	CEUS	2.0
Mueller (2018)	1900	2018	proxy M_w	CEUS	1.0
SLU (Herrmann et al., 2011)	1962	Feb 2023	M_w	CEUS	1.5
TexNet	2017	Feb 2023	M_L	TX	1.0
TexNet Research [1]	2019	2021	M_L	TX	1.0
Frohlich et al. (2016)	1902	2015	varied	TX	3.0
NTXES [2]	Oct 2008	Jul 2021	M_L	north-central TX	-1.3
Oklahoma Geological Survey (OGS)	1983	Feb 2023	$M_L/m_{bLg}/M_w$	OK	1.0
Schoenball & Ellsworth (2017)	May 2013	Nov 2016	varied [3]	OK	0.7
Skoumal et al. (2019) [4]	May 2010	2016	M_L [3]	OK	1.8
Holland (2013)	Jan 2011	Jan 2011	M_L [3]	south-central OK	1.8

[1]extension of the public TexNet catalog that includes earthquakes of limited manual review due to their smaller size
[2]extended version. Includes events from SMU (Quinones et al., 2019), Frohlich et al. (2012), ComCat, Ogwari et al. (2018), Scales et al. (2017), and template-matched unpublished data from Michael Brudzinski.
[3]we used the proxy M_w values already computed by Grigoratos et al. (2020a)
[4]employed template matching with relocations for newly detected events; added 0.38 M_L units to each event following Kavoura et al. (2020)

A.2 Injection data

Our source of wastewater disposal data after 2008 within Texas was the B3 database. At the time of our analyses, it was assumed complete till 2021. That said it also covered 2022, because B3 extrapolates trends from nearby wells in a proprietary way to fill in any gaps. Our analyses required monthly injection rates, the coordinates of the well and in some basins the target-formation. Only wastewater disposal wells were included; Enhanced Oil Recovery (EOR) wells were not taken into account, given that EOR operations aim to stabilize, rather than increase, the pore pressure. The (true vertical) depth was also collected, although not used explicitly, because all our analyses were in 2D.

Our sources of HF data within Texas were the FracFocus Chemical Disclosure Registry and the IHS Markit database. Reporting to FracFocus started in 2011 and became mandatory after January 2012, whereas the IHS Markit database dates back multiple decades and (within TX) is sourced from the Texas Railway Road Commission (RRC).

Our analyses required the start- and end-date of each HF stimulation, the coordinates of the stimulating well, and the average daily injected fluid volume. The latter was obtained by dividing the reported total volumes by the duration of the stimulation. The (true vertical) depth was also collected, although not used, because all our analyses are in 2D. When a frac-job was reported by both FracFocus and IHS, we used dates and volumes from FracFocus and location and depths from IHS. When aggregating the HF volumes into blocks, we used the midpoint between the well's "heel" and "toe.". More details about the HF data are provided in the supplement.

Our pre-processing of the HF data was based on the work of Grigoratos et al. (2022). FracFocus contains one fracture job per entry, with start/end- dates, "Total Base Water Volume" (Volw), "Total Base Non-Water Volume" (Volo), true vertical depth, and surface coordinates for each well. Records from IHS, on the other hand, have multiple entries per fracture job, each with a single date and multiple fluid-types and volumes. We aggregated the IHS entries into fracture jobs merging multi-row entries based on their 14-digit API and reorganized the volumes into the two classes adopted by FracFocus (Volw, Volo). The biggest issue with IHS is the lack of a clear start/end- date for each stimulation. The single date provided is assumed to be the start-date, even though for a significant percentage of the wells this was not the case. Lacking any information on the end-date from IHS, we had to use the injected volume as a proxy for duration. To do that, we used the regression derived by Grigoratos et al. (2022). No meaningful correlation was observed for Volo.

$$\begin{aligned} duration &= 3, && \text{if } Volw < 45000 \text{ bbls} \\ duration &= 19 \cdot log_{10} Volw - 85.4, && \text{otherwise} \end{aligned} \tag{S1}$$

Usually, non-water based volumes (Volo) represent <1% of the total amount. However, according to IHS some TX basins had larger (yet single-digit) percentages, for unknown reasons. That is why we decided to use as total volume the sum of Volo and Volw.

A.3 Equations of earthquake recurrence models

At each block, the null hypothesis, with total likelihood L_0, assumes that all earthquakes are of tectonic origin and is modelled using the classic Gutenberg–Richter (G-R) relationship:

$$\lambda = 10^{a_{tec} - bm} \quad \text{(S2)}$$

where λ is the rate of earthquakes with magnitude larger or equal to m, a_{tec} is the background tectonic activity rate above magnitude 0 (in $\log_{10}$ units) and b is the log–linear slope of the G-R relation (Gutenberg and Richter, 1956).

The alternative hypothesis, with total likelihood L_1, assume a relationship exists between injection and seismicity. It is governed by the following block-specific equations.

$$\lambda[t] = \left(10^{a_{tec}} + v_{lag}[t] \cdot 10^{\Sigma}\right) \cdot 10^{-bm} \quad \text{(S3)}$$

$$t_{lag}[t] = \frac{\theta}{v[t]} \quad \text{(S4)}$$

where t is time (in days or months), Σ is the block-specific Seismogenic Index (Shapiro et al., 2010) and v is the monthly disposal rate for SWD (m^3) or the daily injected volume for HF (m^3). The variable t_{lag} is a proxy for the injection-rate-dependent time-lag between injection and seismicity rate changes. For simplicity, it is assumed to be inversely proportional to v (Grigoratos et al., 2020a), with θ being the factor of (inverse) proportionality. Next, v_{lag} is derived from v and t_{lag} as follows: each monthly/daily value of v is shifted in the future based on the corresponding value of t_{lag} (rounded integer) on that day/month *t*. The two block-specific model-parameters, Σ and θ, are estimated using maximum-likelihood, assuming that each month (or day) the declustered seismicity follows a non-homogeneous Poisson process with varying mean rate $\lambda[t]$ (driven by injection). Finally, given that the time-lag for HF is usually a few days, we also tested (for comparison) a constant time-lag t_{lag}^{c}, which we will treat as a model parameter that replaces equation S4 (only for HF). Given that almost all HF-induced earthquakes happen either during or right after the stimulation (Grigoratos et al., 2022), for the HF analyses we limited both $t_{lag}[t]$ and t_{lag}^{c} to values between 0 and 14 days, to avoid overfitting in the presence of other triggering factors (e.g. SWD).

Apart from the two free-parameters Σ and θ, two other parameters need to be defined a-priori to run the calibration, the b-value and a_{tec}. We should note that the actual b-value used in equations S2 and S3 to estimate λ[t] at M equal to M_c is not critical, as long as the same value is consistently used for the calibration of Σ and θ (or t_{lag}^{c}); we opted for a typical b-value of 1. The value of a_{tec} was set very low given the lack of tectonic seismicity in the region. Our results are not sensitive to the a_{tec} value, because it is usually orders of magnitude smaller than the implied a-value from induced seismicity.

Given that the time-lag for SWD can be months or years, prior injection history is important when modelling a specific time-period (Grigoratos et al., 2020b). Therefore, even though we perform the maximum likelihood regression for Σ, θ (and L_1, L_0) only during time-periods of low M_c, we processed all the available disposal data dating back to 2000 when simulating (for any given value of θ) the time-dependent variable v_{lag}. In other words, the months considered in computing the total maximum likelihood of each block can be a subset of the entire $v_{lag}[t]$ time-series, allowing the user to focus on specific time-periods of interest.

Finally, to simplify things, since we were only interested in the p-values and not in seismicity rate forecasting, we did not implement additional considerations related to the Kaiser effect (Shapiro and Dinske, 2007) in the SWD formulations. The HF formulation never had such considerations to begin with, given how localized the effects of each new stimulation are.

A.4 Distributed SWD volumes

Although the Theis (1935) equation simulates fluid flow and the associated changes in pore pressure (i.e. head), we applied it to the injection volumes because the Seismogenic Index model uses injection volumes as a proxy for changes in pore pressure. Note that, here, the spatial and temporal distributing of the injection volumes is an attempt to model the effects of pore pressure diffusion, and it is distinct from the seismicity time-lag modeled by equation S4.

Given a constant rate of discharge from a well (v in units of m^3/s), the drawdown s (m) as a function of time since the beginning of pumping (t) and radial distance from the well (r) is given by (Theis, 1935):

$$s[r,t] = h_0 - h[r,t] = \frac{v}{4\pi T} \int_{\frac{r^2}{4Dt}}^{\infty} \frac{e^{-u}}{u} du \quad \text{(S5)}$$

where h_0 is the initial fluid head, $h[r,t]$ is the head during pumping, T is the transmissivity (m^2/s) and D is the hydraulic diffusivity (m^2/s). In our application, v is injection rate rather than discharge rate and thus equation 6 provides the increase in head rather than the drawdown. We use equation S5 to distribute the monthly injected volumes spatiotemporally before we utilize them in equation 4. Further implementation details are provided in Grigoratos et al. (2020a).

The only parameter needed to compute the distribution factors is the diffusivity, D. Since the Theis equation describes radial flow within a single layer, we cannot model the effects of the injection layer and the basement separately. Instead, the parameter D represents the large-scale diffusivity that is often derived from seismicity migration analyses (Parotidis and Shapiro, 2004). It is not identical to the diffusivity values often assigned to specific formations. Within Oklahoma the large-scale D value ranges between 0.1 and 2 m^2/s (e.g. Goebel et al., 2017). Grigoratos et al. (2020a) opted for D equal to 0.3

m^2/s. Within the DFW area, and specifically for the Ellenburger formation, Zhai & Shirzaei (2018) opted for a D equal to 0.7 m^2/s, which is the upper value from the range of Hornbach et al. (2015).

Additional references

ComCat. U.S. Geological Survey, Earthquake Hazards Program, 2017, Advanced National Seismic System (ANSS) Comprehensive Catalog of Earthquake Events and Products: Various, https://doi.org/10.5066/F7MS3QZH.

Frohlich, C., Glidewell, J., & Brunt, M. (2012). Location and Felt Reports for the 25 April 2010 mbLg 3.9 Earthquake near Alice, Texas: Was it Induced by Petroleum Production? Bulletin of the Seismological Society of America, 102(2), 457–466. https://doi.org/10.1785/0120110179

Goebel, T. H. W., Weingarten, M., Chen, X., Haffener, J., & Brodsky, E. E. (2017). The 2016 Mw 5.1 Fairview, Oklahoma earthquakes: Evidence for long-range poroelastic triggering at >40 km from fluid disposal wells. Earth and Planetary Science Letters, 472, 50–61. https://doi.org/10.1016/j.epsl.2017.05.011

Gutenberg, B., and Richter, C.F. (1956). Earthquake magnitude, intensity, energy, and acceleration: (Second paper), Bull. Seismol. Soc. Am. 46(2), 105-145.

Herrmann, R.B., Benz, H. and Ammon, C.J. (2011). Monitoring the earthquake source process in North America, Bull. Seismol. Soc. Am., 101, 2609–2625, doi:10.1785/0120110095

Holland, A. A. (2013). Earthquakes Triggered by Hydraulic Fracturing in South-Central Oklahoma. Bulletin of the Seismological Society of America, 103(3), 1784–1792. https://doi.org/10.1785/0120120109

Kavoura, F., Savvaidis, A., & Rathje, E. (2020). Determination of Local Magnitude for Earthquakes Recorded from the Texas Seismological Network (TexNet). 13.

Mueller, C.S. (2018). Earthquake catalogs for the USGS National Seismic Hazard Maps. Seismological Research Letters, 90(1), 251-261.

Parotidis, M., & Shapiro, S. A. (2004). A statistical model for the seismicity rate of fluid-injection-induced earthquakes. Geophys. Res. Lett. 31(17).

Schoenball, M., and Ellsworth, W.L. (2017). A systematic assessment of the spatiotemporal evolution of fault activation through induced seismicity in Oklahoma and southern Kansas, J. Geophys. Res. Solid Earth. 122(12).

Shapiro, S. A., & Dinske, C. (2007). Violation of the Kaiser effect by hydraulic-fracturing-related microseismicity. Journal of Geophysics and Engineering, 4(4), 378–383. https://doi.org/10.1088/1742-2132/4/4/003

Skoumal, R. J., Kaven, J. O., & Walter, J. I. (2019). Characterizing Seismogenic Fault Structures in Oklahoma Using a Relocated Template-Matched Catalog. Seismological Research Letters. https://doi.org/10.1785/0220190045

Walter, J. I., Ogwari, P., Thiel, A., Ferrer, F., Woelfel, I., Chang, J. C., Darold, A. P., & Holland, A. A. (2020). The Oklahoma Geological Survey Statewide Seismic Network. Seismological Research Letters, 91(2A), 611–621. https://doi.org/10.1785/0220190211

Supplemental figures and tables

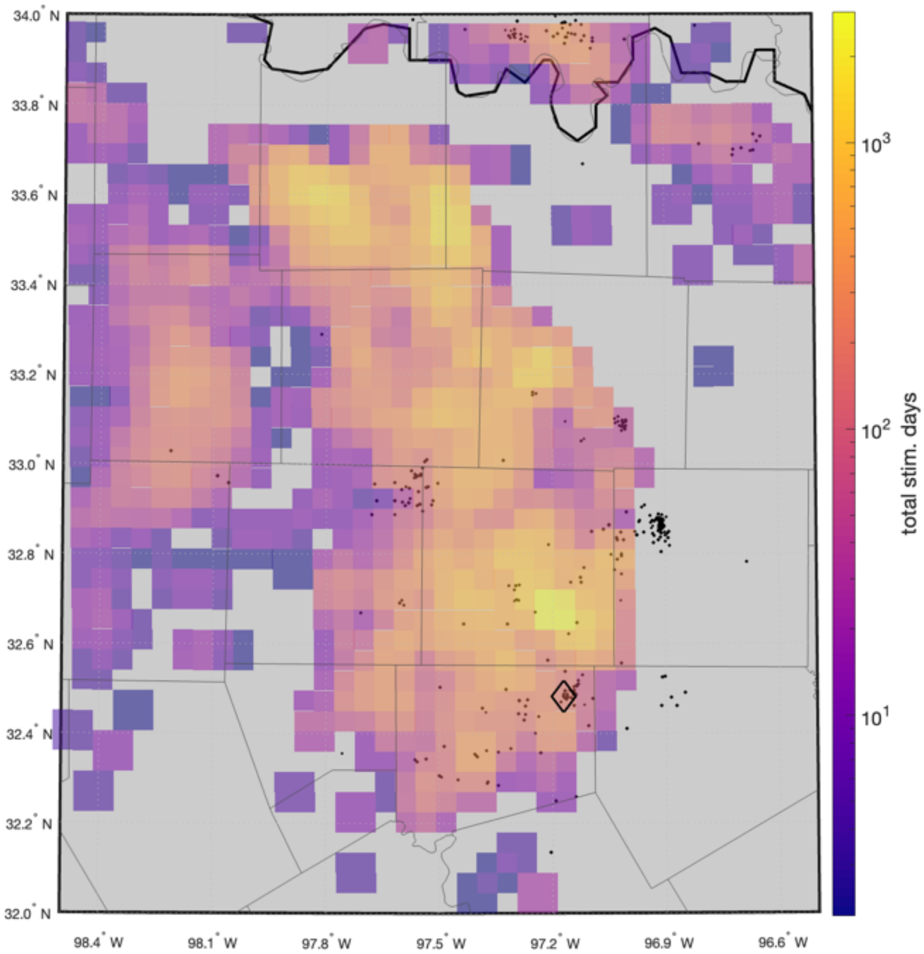

Figure S1. Map of the given investigated area showing declustered seismicity (M ≥ 2; black dots), gridded cumulative HF stimulation-days and county/state borders. The black diamond indicates the M_w 4.0 Venus earthquake. Data between 2008 and September 2022.

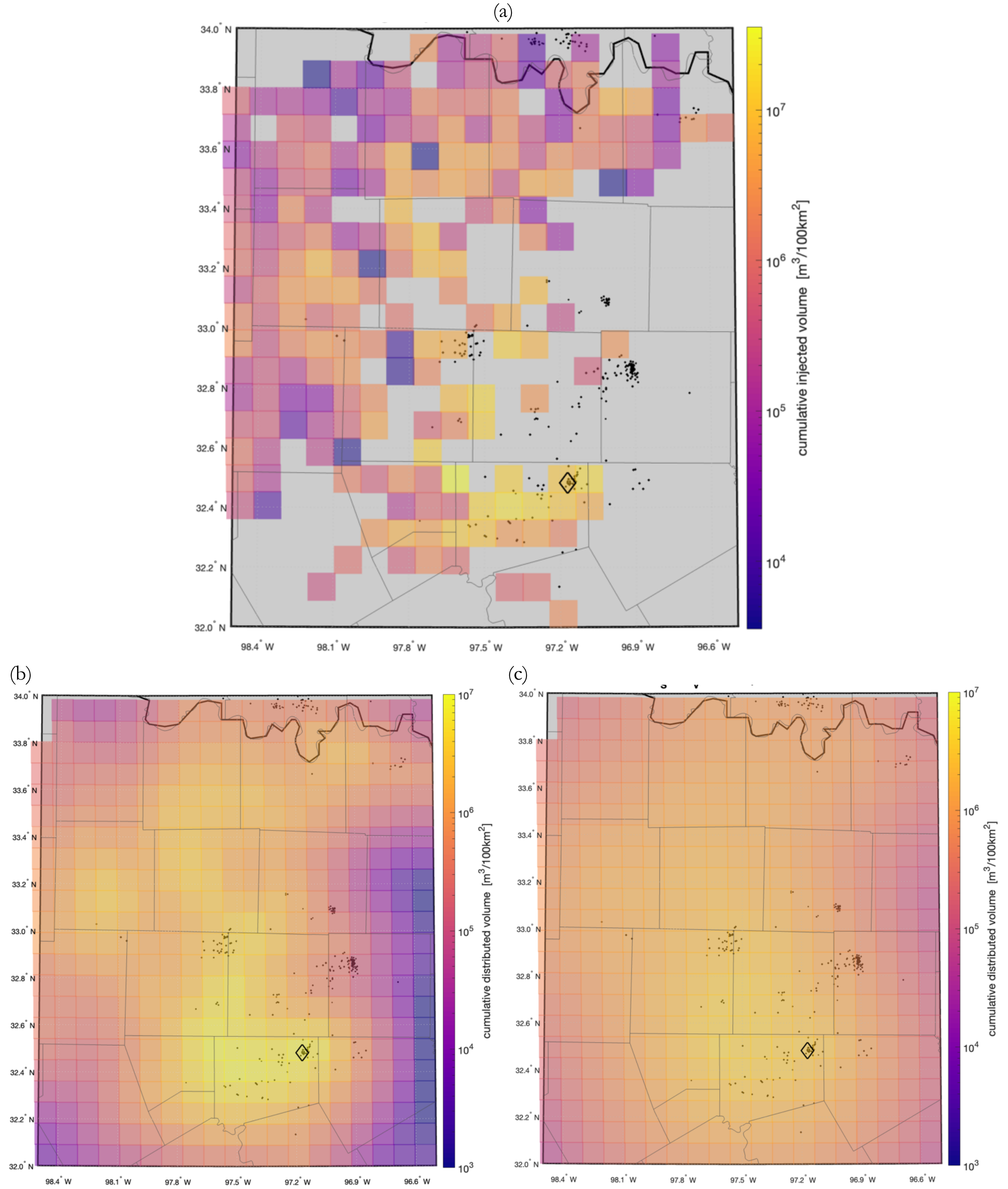

Figure S2. Map of the investigated area showing declustered seismicity (M ≥ 2; black dots), gridded cumulative injected (a) or diffused SWD volumes (b,c). The large-scale diffusivity (D) value is 0.3 in (b) and 2 m^2/s in (c) The black diamond indicates the M_w 4.0 Venus earthquake. Data between 2006 and 2021. County/state borders are also mapped.

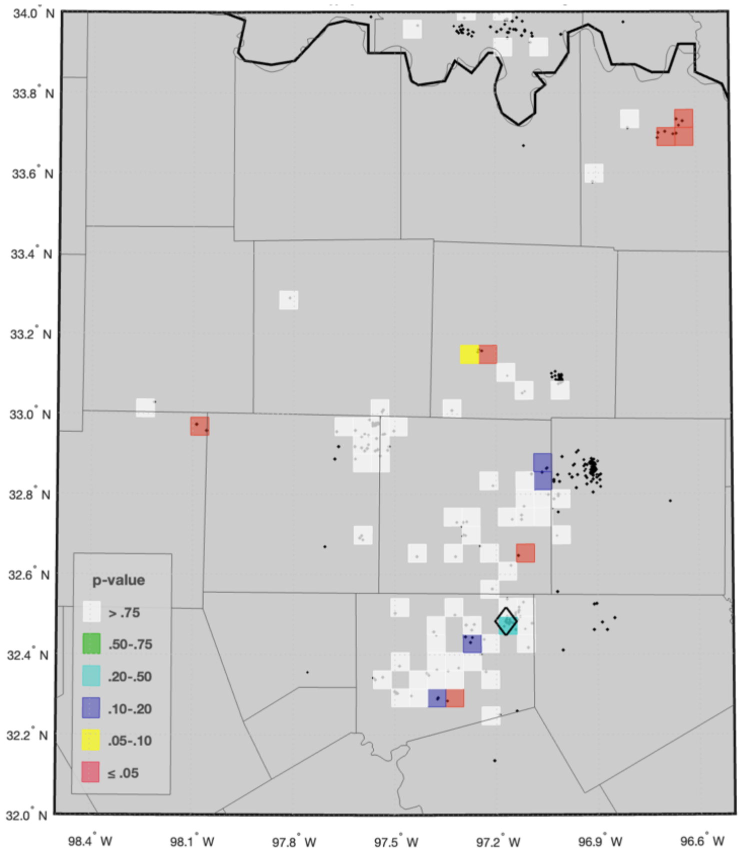

Figure S3. Same as Figure 3, but using the non-declustered catalog.

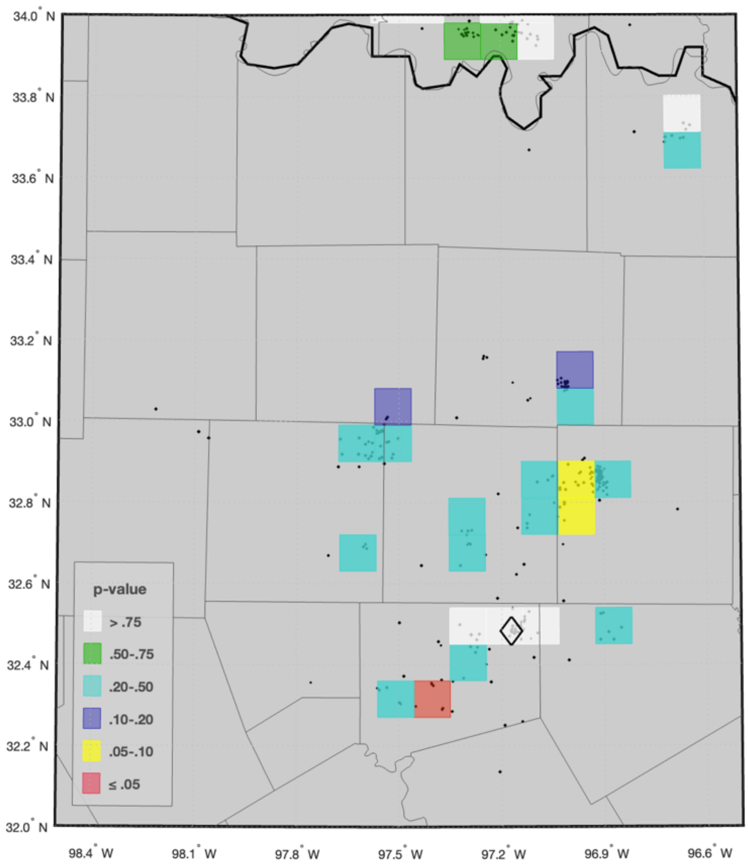

Figure S4. Same as Figure 4, but for D = 1 m^2/s.

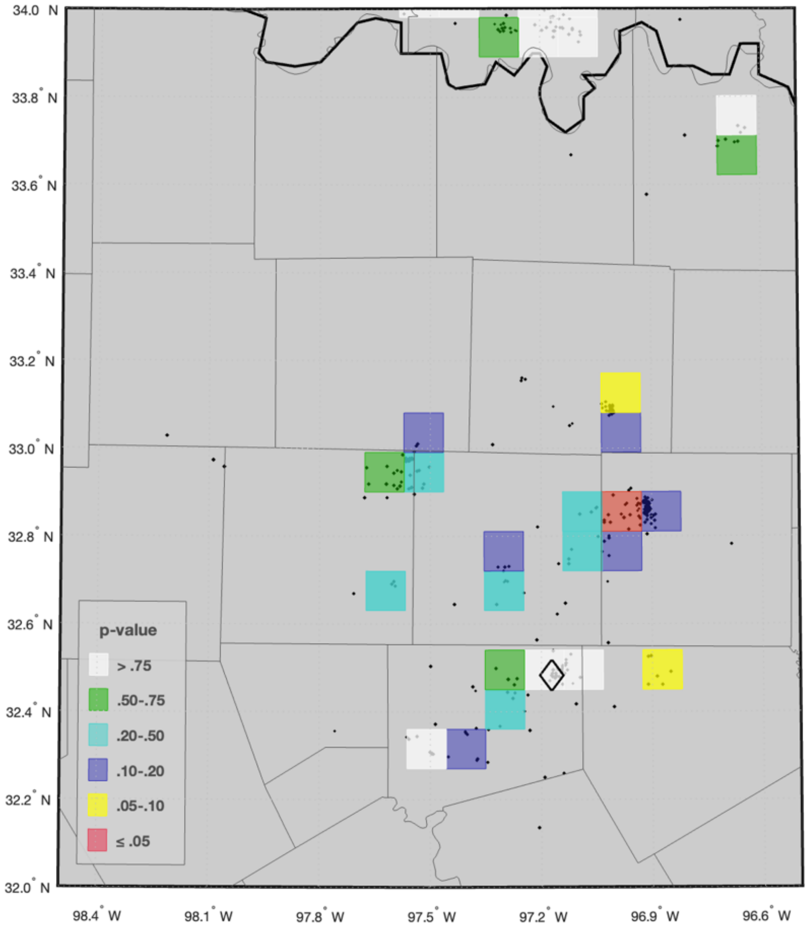

173
174 Figure S5. Same as Figure 4b (D = 2 m²/s), but for the non-declustered catalog.